10-11 (2024) 100029

Contents lists available at ScienceDirect

IPEM-Translation

journal homepage: www.elsevier.com/locate/ipemt

Full Length Article

The use of solar film elements on a neonate manikin surface to estimate the received output power of neonatal phototherapy lamp systems

D.M. Clarkson [a,1,*], P. Satodia [b]

[a] Department of Research and Development, University Hospital Coventry, Coventry, CV2 2DX, UK
[b] Neonatal Intensive Care Unit, University Hospital Coventry, Coventry, CV2 2DX, UK

ARTICLE INFO

Keywords:
Neonatal phototherapy
Bilirubin
Neonatal jaundice
Amorphous silicon

ABSTRACT

The work described was undertaken to develop a means to estimate the delivered power over the exposed body surface of a neonate receiving phototherapy. Previous work of the group had involved the use of discrete photodiodes distributed over a newborn manikin surface. It was considered that improved accuracy of sensing over curved surfaces would be provided with the use of flexible solar cell elements. A group of products based on amorphous silicon was identified as potentially suitable and a range of its properties investigated. These included the wavelength sensitivity, the relative sensitivity of similar elements and the cosine response of elements. It was identified that with selection of elements of matched sensitivity, specific element types were appropriate for intended use. A total of 44 discrete solar cell elements of three separate sizes was used to cover the previously used manikin surface and a dedicated interface circuit was designed and constructed. A handheld calibrated spectroradiometer provided a means to relate incident irradiance values within specific wavelength bands to corresponding optical power over the manikin surface. Initial use of the system is described together with future potential developments in relation to clinical applications and testing standards for neonatal phototherapy devices.

1. Introduction

Our group [1] previously introduced a new technique to estimate the optical power of a neonatal phototherapy source within specific wavebands. This was identified as a key development to aid the effectiveness of this therapy; as the system could be used to optimise the dose rate delivery over the neonatal surface. The previous system had utilised 192 discrete photodiode detectors which were grouped into 12 anatomical areas on the surface of a specific newborn manikin, Newborn Anne (Laerdal Medical AS, Stavanger, Norway). This surface profile is subsequently referenced as the 'babyshape'. It was identified, however, that improvements in detection technology were desirable to increase accuracy of detection of light over curved surfaces and that flexible solar film elements provided a potentially suitable alternative. It was also considered relevant to reduce the number of actively monitored channels to simplify measurement processes and which was achieved by connecting solar film elements in parallel within a given anatomical area. The use of flexible amorphous silicon film detectors is subsequently described and which initially involved detailed investigation of their detection properties.

2. Materials and methods

2.1. Identification of suitable solar film elements

A source of solar film elements based on amorphous silicon technology (PowerFilm Solar, Ames, IA, USA) was identified as potentially suitable for the application and properties of specific elements primarily designed for energy conversion of indoor light sources were investigated. It was identified that the basic measurement parameter of such elements was that of the effective generated short circuit current, with the element behaving like a current generator. The key properties investigated of these solar film elements included the wavelength sensitivity of individual elements, the degree of uniformity of light sensitivity within a set of similar elements, the cosine response of elements and the demonstration that the sum of currents from linked elements in parallel was equivalent to the sum of the response from individual elements.

* Corresponding author.
E-mail address: douglas.clarkson@uhcw.nhs.uk (D.M. Clarkson).
[1] (DM Clarkson) is given as 'University Hospitals Coventry and Warwickshire NHS Trust'.

https://doi.org/10.1016/j.ipemt.2024.100029
Received 29 December 2023; Received in revised form 10 May 2024; Accepted 14 June 2024
Available online 27 June 2024
2667-2588/© 2024 The Author(s). Published by Elsevier Ltd on behalf of Institute of Physics and Engineering in Medicine (IPEM). This is an open access article under the CC BY-NC-ND license (http://creativecommons.org/licenses/by-nc-nd/4.0/).

Table 1
Details of current and previous measurements of 'babyshape' anatomical area and number of solar elements used in revised system.

Anatomical area	Current determined area (cm^2)	Previously determined area (cm^2)	Number of solar elements	Element reference
Head/neck (rear)	177.1 ± 2.7	271.3 ± 4.1	6	LL200–2.4–37
Head/neck (front)	315.3 ± 4.7	271.3 ± 4.1	10	LL200–2.4–37
Upper torso (left)	154.4 ± 2.3	165.7 ± 2.5	3	LL200–4.8–37
Upper torso (right)	158.0 ± 2.4	165.7 ± 2.5	3	LL200–4.8–37
Rear torso (left)	195.8 ± 2.9	209.8 ± 3.2	3	LL200–4.8–37
Rear torso (right)	203.7 ± 3.1	209.8 ± 3.2	3	LL200–4.8–37
Left leg upper	173.9 ± 2.6	173.3 ± 2.6	4	LL200–4.8–37
Right leg upper	177.2 ± 2.7	173.3 ± 2.6	4	LL200–4.8–37
Left arm	163.7 ± 2.5	168.1 ± 2.5	2	LL200–4.8–37
Right arm	176.0 ± 2.6	168.1 ± 2.5	2	LL200–4.8–37
Left leg lower	159.3 ± 2.4	173.3 ± 2.6	2	LL200–3–37
Right leg lower	176.4 ± 2.7	173.3 ± 2.6	2	LL200–3–37
Total	**2230.8** ± 33.6	**2323.0** ± 35.0	**44**	

2.2. Review of anatomical areas

Use was made of the previously utilised Newborn Anne manikin and the same defined set of anatomical areas was utilised, though the boundaries of various of these were modified to reflect the use of the solar film detecting elements. It had been previously identified [2,3] that the surface area of the NewBorn Anne manikin as measured using low tack masking tape matched that of predicted values of term neonates based on representative values of weight and length of neonates. The method of determining these areas was to attach low tack masking tape to the various surfaces and then sum the areas of attached tape elements when removed. The uncertainty in determined values of anatomical area was estimated from repeated measurements of a cone frustum section over its curved surface and smaller circular area. This indicated a likely error of ± 1.5 % for the technique involving masking tape.

Table 1 indicates the updated surface area measurements and the set obtained previously together with details of the allocated solar film elements. Fig. 1 indicates the three element types used.

2.3. Solar cell detection circuits and interface design

It was identified that a range of different sizes of solar film elements would be required to cover the 12 anatomical areas of the 'babyshape' and that each anatomical area would use a common solar film element. This led to the identification of the role of a separate 'calibration pod' to characterise the responses of elements used in the main 'babyshape' unit and where up to six such elements in the 'calibration pod' could be utilised. This allowed the calibration of groups of elements in anatomical areas of the 'babyshape' to be referenced to a specific single element in the 'calibration pod'. As part of the calibration process, a 'calibration pod' element would be exposed to a known irradiance value from the neonatal phototherapy lamp being measured. In addition, two temperature sensors of type LMT86 (Texas Instruments, Dallas, TX, USA) were located on the 'babyshape' and one on the 'calibration pod'. This allowed temperature differences between the two units to be monitored. Calibration of these sensors was undertaken using a Testo 103 thermometer unit (Testo SE & Co. KGaA, Titisee, Germany).

Use was made of INA122PA instrumentation amplifiers and 10 ohms precision resistors to detect output current values from solar elements as outlined in Fig. 2. Selectable gain was configured by use of combinations of switches Sw1, Sw2 and Sw3 and with maximum gain of 105 set with value of Rg2 of 2k ohms. Values of Rg1 and Rg3 of 4 k ohms and 8 k ohms when individually selected would result in gains of 55 and 30 respectively. Voltage lines of ±5 V were regulated from 9 V battery supplies. A double sided circuit board of dimension 27 by 34 cm was designed using EASYPC software (Number One Systems, Tewksbury, UK) and manufactured by Newbury Electronics (Newbury, UK). Analogue outputs from the interface were switched in two sets of 16 lines by means of 8 manually operated DPST switches to the interface output port which was connected to a USB-1616FS interface device (National Instruments, Austin, TX, USA) with voltage measurement resolution of 305 μV. The use of physical switches was selected to avoid the introduction of additional signal noise with use of analogue

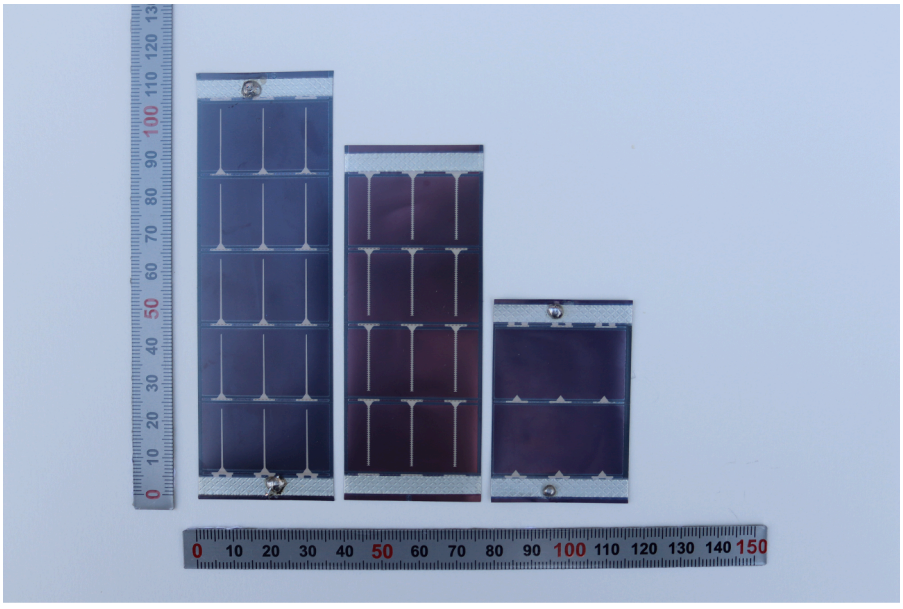

Fig. 1. The three types of solar cell element used (left to right) on the 'babyshape': LL200–3–37 (lower legs); LL200–4.8–37 (torso, upper legs and arms); LL200–2.4–37 (head).

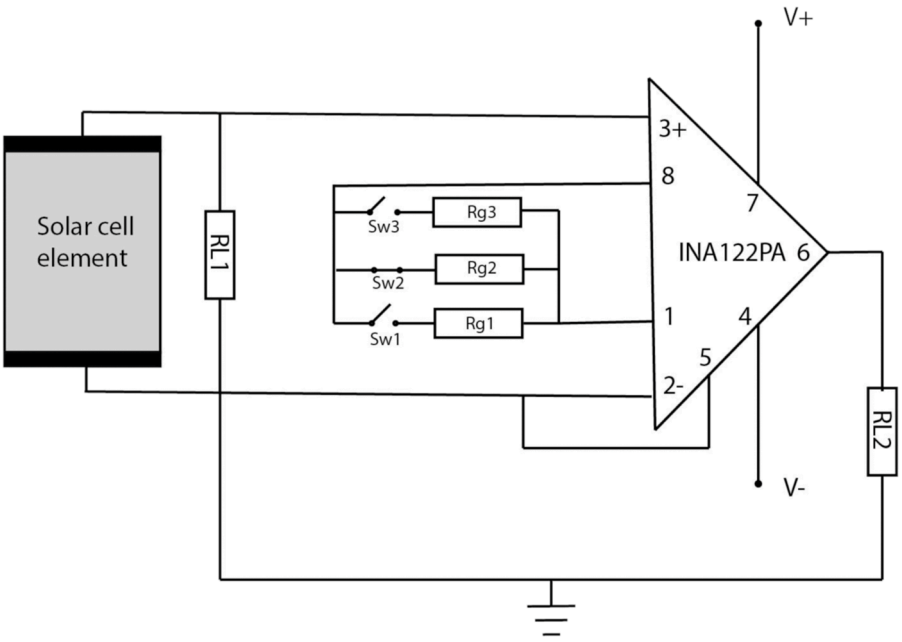

Fig. 2. Solar film connections to INA122PA instrument amplifier.

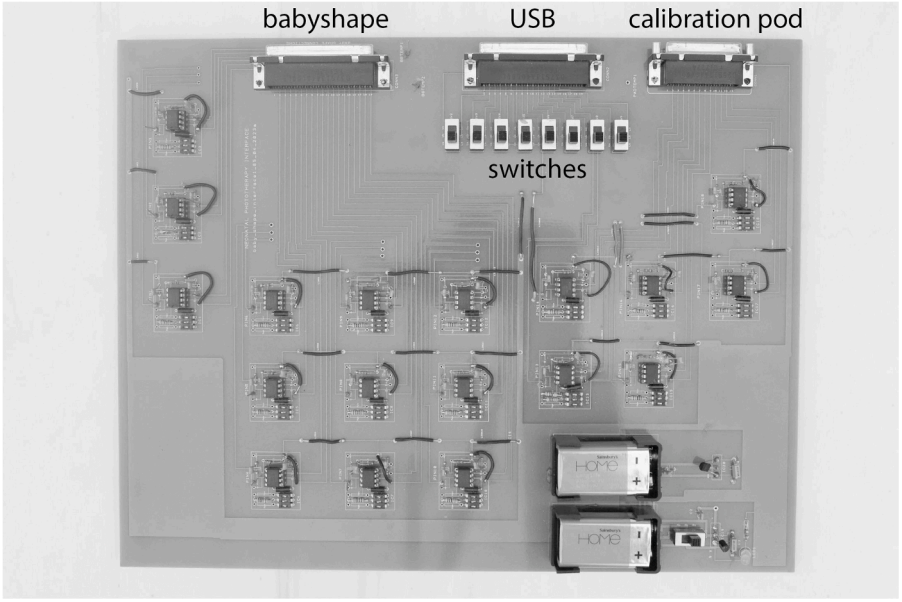

Fig. 3. Image of completed interface system.

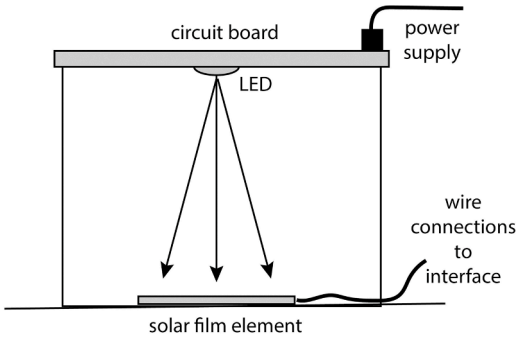

Fig. 4. Detail of LED light source configuration used to determine relative solar element sensitivity.

multiplexing circuitry. Data of each measurement set from the USB interface was captured on a laptop PC at 100 Hz rate and 100 sample values directly into Excel files. The completed interface is indicated in Fig. 3.

2.4. Determination of solar element characteristics

A range of separate high power LEDs with centre wavelengths of 460.3 nm, 516.3 nm, 591.6 nm, 613.1 nm and 628.2 nm and typical full width half maximum (FWHM) value of 30 nm was fabricated based on a cylindrical plastic section of 10 cm inner diameter and height 7.5 cm above the solar film element being tested as indicated in Fig. 4. This would provide information relating to the wavelength response of the solar film elements. The LED centred at 460.3 nm was used to determine the relative response of solar film elements since it matched

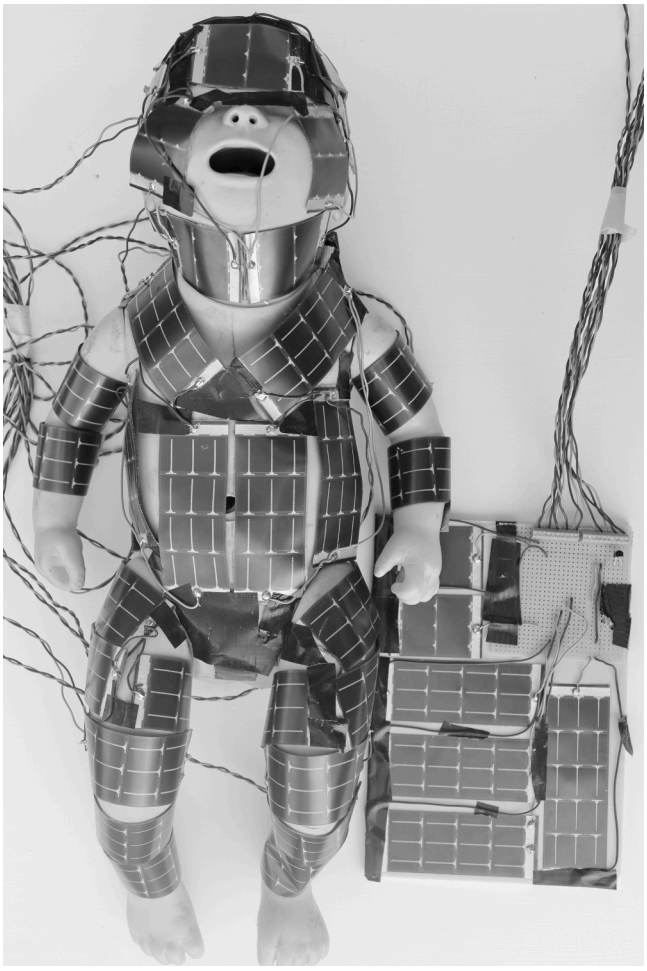

Fig. 5. Image of 'babyshape' covered with solar film elements together with 'calibration pod'.

appropriately to the wavelength outputs of typically available neonatal phototherapy lamp systems.

Solar film elements of a given type were allocated unique identification numbers to assist in element selection/traceability for both the 'babyshape' and the 'calibration pod'.

2.5. Determination of cosine response of solar cell elements

A open sensing area of 4.0 cm diameter on an LL200–3.6–75 PowerFilm solar film element was placed 70 cm below an LED light source on a rotating surface whose angle of inclination was determined using a rotary potentiometer (10 kohms; 285° rotation) and which was driven by a 2.5 V reference source. The detected element signal was amplified using an INA126PA instrument amplifier. The demonstration of a cosine response is an important consideration to ensure that the light incident at an angle Φ to a vertical line from an element surface is detected as the cosine of angle Φ.

2.6. Parallel connection of solar elements

Based on models of photovoltaic cells [4] with identified elements of shunt resistance and diode in parallel with current generator, it was important to verify that the sum of currents from linking elements in parallel was equivalent to the sum of the response from individual elements. The linking of elements in parallel also reduced significantly the number of active measurement channels.

Using an overhead LED lamp source and specific interface channel #13, measurements were made of separate output voltages referenced to zero light input from solar film elements used in the head (6 elements), torso (6 elements) and lower leg (3 elements).

2.7. Identification of correction factors

A specific correction factor was identified to account for differences in average grouped sensitivity of elements in an anatomical area compared with the allocated solar film element in the 'calibration pod'. Where different gains are established between a calibration channel i and a 'babyshape' channel j, the corresponding gain correction factor for channel j is given by the ratio of gain of channel i divided by that of channel j. Gain resistor values could be selected by means of switches Sw1, Sw2 and Sw3 on the main interface circuit to prevent channel saturation.

Fig. 6. Image of CSS-45-Bili detection unit with CSS-D console display unit.

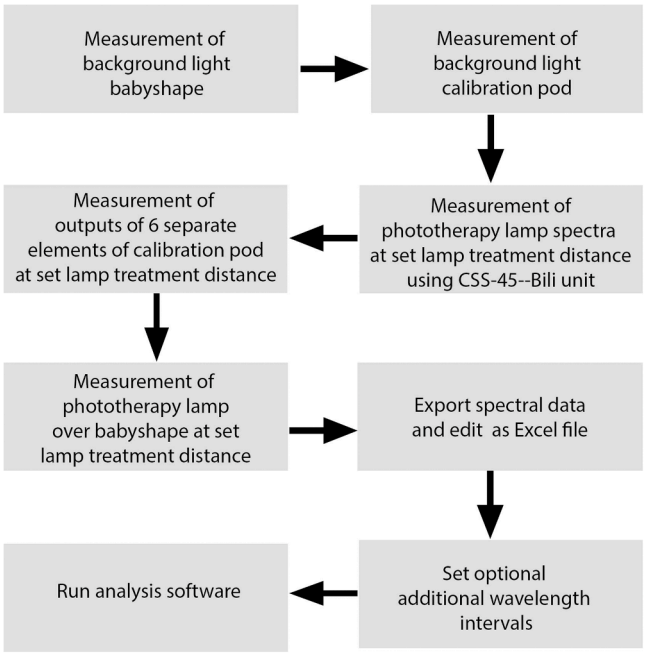

Fig. 7. Summary of measurement process.

2.8. Construction of 'babyshape' and 'calibration pod'

Based on element sensitivity responses obtained using the 460.3 nm LED light source, solar film elements were grouped to provide close matching of sensitivity values between 'babyshape' anatomical areas and a corresponding calibration element of the same type on the 'calibration pod'. When wires were soldered to the connecting edges of the solar elements, the main sensing surface was sandwiched between thin metal plates to minimise temperature elevation of the solar film element. The use of low temperature solder would also be a sensible precaution. The use of conductive adhesives was considered, though it was identified that use of solder contacts would probably provide greater reliability of connection. Use was made of transparent double sided adhesive tape (Scotch-Fix™ Transparent Mounting Tape, 3 M, Saint Paul, MN, USA) to attach elements to the 'babyshape' surface. Fig. 5 indicates the 'babyshape' together with the 'calibration pod'.

2.9. Spectral measurements

It had previously been identified [5] that an underlying problem with effective output measurements of neonatal phototherapy lamps had been the lack of traceable calibrations of output meters. It was subsequently indicated [6] that the use of an MSC-15 handheld spectroradiometer (Gigahertz Optik GmbH, Türkenfeld, Germany) was appropriate to characterise the output of such lamp systems. Use was made of a more recently available equivalent unit comprising a CSS-45-Bili detector with CSS-D console (Gigahertz Optik GmbH, Türkenfeld, Germany) interfaced to a PC. This unit, indicated in Fig. 6, had the advantages of auto dark current calibration and a detachable sensor with improved cosine response. Traceability of measurements was ensured by accreditation of Gigahertz Optik GmbH to ISO/IEC 17,025. Spectral data was available between 360 nm and 830 nm at 1 nm intervals and the spectral parameters identified in reports of the American Academy of Pediatrics [7,8] as AAP2004 and AAP2011 were automatically calculated by the unit with reference to 60 nm and 30 nm wavelength extents respectively. Comprehensive spectral data and associated derived parameters to support a range of technical and scientific applications were exported as text files and converted to Excel format for subsequent analysis.

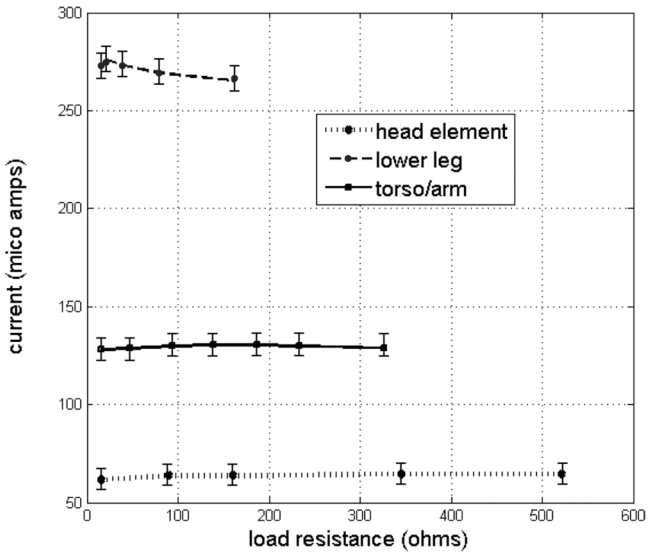

Fig. 8. Calculated current value for varying resistance load values with three solar film element types based on a nominal gain of 105 of the instrument amplifier using the 460.3 nm centre wavelength LED source.

The relative uncertainty in spectral irradiance in wavelength range 400 nm to 759 nm is referenced as ±4 % and with the wavelength uncertainty identified as ± 1 nm. The contribution of irradiance error associated with wavelength accuracy within a specific wavelength range was identified as determined by the magnitude of the change of irradiance with wavelength across the defining limits of the indicated wavelength interval.

2.10. Process of neonatal lamp measurements

Fig. 7 outlines the process for measurement of optical power detected on the 'babyshape' surface. Once the basic set of calibration details had been captured using the 'calibration pod', it was only necessary to capture the data sequence from the 'babyshape' system itself when, for example, moving the lamp system relative to the 'babyshape' system. Calibration of the system using the 'calibration pod' required to be repeated at each separate phototherapy output level setting since changing current levels of LEDs would subtly alter the associated spectral output.

Software was written using MATLAB (MathWorks, Natick, MA, USA) to process the various sets of data and create the output report of power in mW detected over the various anatomical areas with reference to the AAP2004 and AAP2011 wavebands. In addition two user defined wavelength ranges could be identified in the software analysis for comparable computation. Measurements were undertaken with the 'babyshape' and 'calibration pod' resting on a white reflective surface.

2.11. System equations

For a specific 'calibration pod' element j, a term Sens_irr(j) is defined as the value in mW cm^{-2} V^{-1} derived from a given net irradiance irrad(j), and net voltage signal PodV(j) where net values are referenced to background light levels.

$$Sens\_irr(j) = irrad(j)/PodV(j) \quad (1)$$

The mean adjusted voltage from a 'babyshape' channel i, Mean_BSV (i), is given by:-

$$Mean\_BSV(i) = Vanat(i)\ Corr(i,j)\ /N\_elements(i) \quad (2)$$

where Vanat(i) is the detected voltage of elements in parallel, Corr(i,j) is a correction factor for amplifier gain and relative sensitivity of calibra-

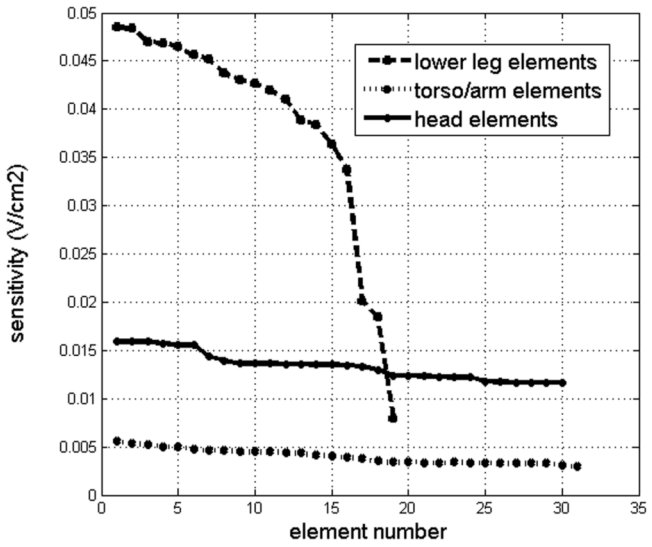

Fig. 9. Details of relative sensitivity of solar film elements used on the 'babyshape'.

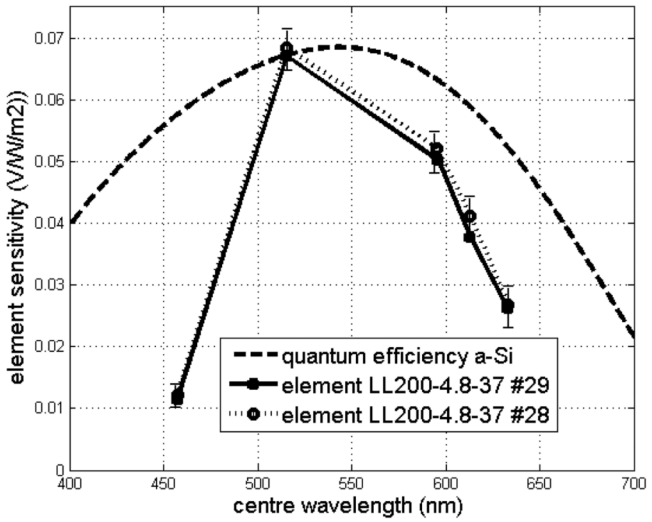

Fig. 10. Determined spectral sensitivity in V /(W/m2) of two similar solar film elements (LL200–4.8–37) with reference to manufacturer's data of quantum efficiency of amorphous silicon.

tion and sensing elements and N_elements(i) is the number of similar film elements in the anatomical area.

The derived output power in mW, Power_mW(i) from an anatomical area Anat_Area(i) is given by:-

$$Power\_mW(i) = Sens\_irr(j)\ Anat\_Area(i)\ Mean\_BSV(i) \quad (3)$$

3. Results

3.1. Observations of value of RL1

Fig. 8 indicates how the calculated value of detected current varied with the value of RL1 in Fig. 2 for a given level of light exposure using the 460.3 nm centre wavelength LED light source. This shows that the detected current is essentially constant as a function of load resistance RL1 for the range of resistance values utilised and that the 10 ohms value for the load resistance was appropriate. An observation with the use of value of 105 instrument amplifier gain is that the maximum detected voltage across the load resistance is around 50 mV before the unit saturates at around 5 V output.

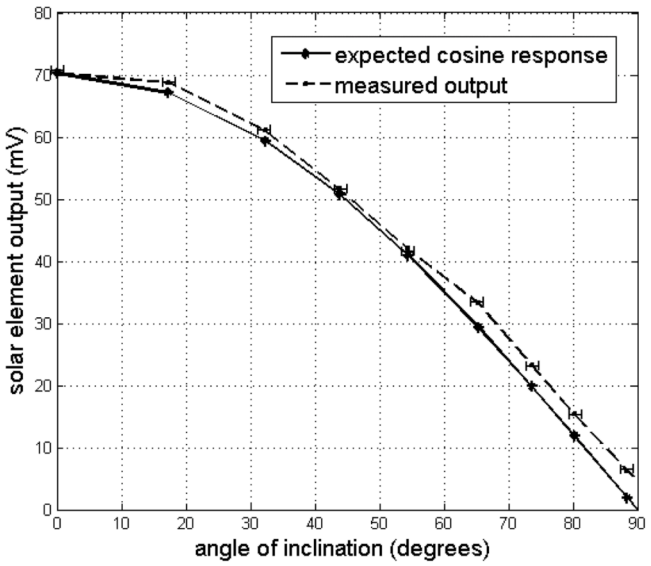

Fig. 11. Observation of detected voltage as a function of angle of inclination of solar film element to the horizontal (cosine response).

3.2. Determination of element sensitivity values

Significant variations in element sensitivity of a specific type were, however, observed within batches of product as outlined in Fig. 9 and linked to aspects of material production where there was no defined range of product sensitivity. This indicated that it was necessary to select elements of a given type for a given anatomical area with similar sensitivity values and also match with the corresponding allocated element in the 'calibration pod'. In addition, it was not appropriate to mix different types of elements within a given anatomical area, due to the variation of sensitivity per unit area between element types.

3.3. Wavelength response of solar elements

The set of LED light sources was used to determine the wavelength response of the solar elements over a range of wavelengths as indicated in Fig. 10. This indicated that the wavelength response of the specific solar film element was narrower than would be suggested by the manufacturer's data of quantum efficiency of amorphous silicon. There was observed, however, a similar wavelength response of the two elements investigated.

3.4. Cosine response of solar elements

Fig. 11 confirms an essentially cosine response of the element investigated and where a component of detected output voltage at angles above 60° is probably due to detected scattered light from the overhead light source.

3.5. Parallel connection of solar film elements

The corresponding percentage differences between net parallel measurements and the sum of net separate measurements at nominal gain level of 105 was observed as $(0.57 \pm 0.41)\%$, $(-1.57 \pm 0.76)\%$ and $(-0.14 \pm 0.66)\%$ respectively for the head, torso and lower leg elements and with uncertainties assessed from consideration of voltage measurement resolution. These deviations were not considered significant enough to be included in correction factors in analysis software.

Table 2
Channel allocations between anatomical areas and linked 'calibration pad' elements; correction factor for element sensitivity and also estimated percentage of active sensing area.

Babyshape anatomical area	Interface input channel	Calibration Channel/ (size)	Sensitivity correction factor	Percentage of active sensing area
Head/neck (rear)	1	14 (small)	0.986	43.7
Head/neck (front)	2	17 (small)	1.03	41.0
Front torso (left)	3	18 (medium)	0.967	47.6
Front torso (right)	4	18 (medium)	1.021	46.5
Rear torso (left)	5	13 (medium)	0.985	37.5
Rear torso (right)	6	13 (medium)	1.038	36.1
Left leg upper	7	16 (medium)	1.002	56.2
Right leg upper	8	16 (medium)	0.998	55.3
Left arm	9	16 (medium)	1.001	29.9
Right arm	10	16 (medium)	0.997	27.8
Left leg lower	11	15 (large)	0.997	38.5
Right leg lower	12	15 (large)	1.006	34.7

Table 3
Detected power in mW over the 'babyshape' in AAP2004 and AAP2011 wavebands and where values in brackets are corresponding values per unit of area in units of mW cm-^{2}.

Babyshape Anatomical area	Output power mW AAP2004 (430 nm –490 nm)	Output power mW AAP2011 (460 nm – 490 nm)
Head/neck (rear)	19.2 ± 2 (0.11)	13.6 ± 1.4 (0.08)
Head/neck (front)	164.5 ± 17.3 (0.52)	115.9 ± 12.2 (0.37)
Front torso (left)	214.4 ± 22.5 (1.39)	151.2 ± 15.9 (0.98)
Front torso (right)	185.4 ± 19.4 (1.17)	130.7 ± 13.7 (0.83)
Rear torso (left)	15.2 ± 1.6 (0.08)	10.7 ± 1.1 (0.06)
Rear torso (right)	14.3 ± 1.5 (0.07)	10.1 ± 1.1 (0.05)
Left leg upper	80.5 ± 12.5 (0.46)	56.7 ± 8.8 (0.33)
Right leg upper	56.7 ± 8.8 (0.32)	40.0 ± 6.2 (0.23)
Left arm	95.7 ± 14.8 (0.58)	67.5 ± 10.5(0.41)
Right arm	76.4 ± 11.8 (0.43)	53.9 ± 8.4 (0.31)
Left leg lower	77.2 ± 12.0 (0.49)	55.5 ± 8.6 (0.34)
Right leg lower	52.0 ± 8.1 (0.30)	36.7 ± 5.7(0.21)
TOTAL	**1051.5** ± 132.3±	**742.5** ± 93.6

3.6. Summary of element sensitivity correction factors and active sensing areas

Details of allocated solar cell elements of the various anatomical areas and links to calibration channels are outlined in Table 2. The areas with the greatest percentage of active detecting surface were the left and right upper leg. It was identified that on average only around 41 % of an anatomical area of the 'babyshape' surface was actually covered by the active sensing area of the utilised solar film elements. In the previous implementation using discrete photodiodes, less than 1 % of 'babyshape' surface had been covered with active light sensing elements. There is an obvious advantage in covering as much as possible of the 'babyshape' surface with active sensing elements to reduce uncertainty of dose rate estimates.

There is also the consideration of light capture symmetry, in particular from overhead and reverse light directions. The head areas and upper and lower torso areas reflect appropriate symmetry of light capture from both directions, though there was an observed preference for overhead detection on upper legs and arms which is being addressed by the use of the smaller solar film element on these anatomical areas. For measurements from blanket light sources, the majority of light will be detected by the rear torso elements.

It was identified that there are limitations in the percentage of active sensing area and degree of light capture symmetry with use of rectangular/square solar film elements. In an ideal configuration, a light sensing element would closely contact the complete surface profile of an anatomical area and demonstrate a uniform light sensitivity factor. Also, the design of a representative 'babyshape' as described in Section 4.5 could significantly increase the percentage of active sensing area.

3.7. Estimation of 'babyshape' delivered power levels

Table 3 indicates the specific observations of a Natus NeoBLUE (Natus Medical Inc., Middleton, WI, USA) lamp system, with peak therapeutic wavelength at 464 nm and with reduced background illumination from LEDs at centre wavelength 594 nm and which was achieved by placing masking tape over their surfaces and which would have reduced also the detected output of the therapeutic wavelengths.

A component of measurement error was associated with the partial surface coverage of the 'babyshape' with solar film elements where the technique assumed that the average irradiance detected by active sensing elements would be present over the non-sensing areas of the particular anatomical area. Values of ± 5 % were identified for this factor over head and torso areas and ± 10 % for arm and leg areas.

The various anatomical areas identified on the 'babyshape' identify an idealised representation of the actual surface areas of the neonate receiving effective phototherapy. The wearing of eye protection will reduce the component received by the front of head and the presence of hair will reduce the component of the rear head. The wearing of a nappy will reduce the components relating to the front and rear torso components. Other restrictions of exposure may also apply. A standard correction profile was included in the analysis software and in addition, a user configured Excel file provided an additional option to refine estimated parameters.

It was apparent that the degree of curvature of the arms and legs limits the useful contribution to delivered power from both overhead and blanket sources while the upper and lower torso areas with a greater extent of flat surfaces have the benefit of higher relative light capture. A useful derived parameter of an anatomical area is that of the 'effective' average irradiance value obtained by dividing the derived incident power in mW by the corresponding surface area and which is indicated in brackets in Table 3. This observation indicated the potential benefit of 'wrap round' light delivery devices in particular for the legs of the neonate. In the example of AAP2011 criteria and using the data in Table 3, if the legs could demonstrate an equivalent 'effective' irradiance value to the highest value of that of the upper torso of 0.98 mW cm $^{-2}$, then this would increase the total delivered power to the neonate by around 65 %. The testing of additional neonatal lamp systems is ongoing.

4. Discussion

4.1. Role of amorphous silicon

Amorphous silicon has characteristics which differ from those of crystalline silicon. The absorption thickness is typically around 1 μm compared with around 100 μm for the crystalline form, though the conversion efficiency is at best around 8 % compared with current typical values of less than 23 % for the crystalline form [9]. Amorphous silicon, however has a lower temperature coefficient of around - 0.25 % per °C increase in temperature. Amorphous silicon, however, is known to reduce in efficiency over a period of exposure to solar radiation of around 10 % to 15 % after which it demonstrates relative stability. This effect is known as the Staebler-Wronski effect [10,11]. The exposure of the amorphous silicon solar elements to levels of ambient light levels

likely to be experienced in use would be significantly less than in bright sunshine, though as a precaution the 'babyshape' and 'calibration pod' were screened from light when not in active use. Further work is ongoing to monitor changes in solar film element efficiency as a function of exposure to specific levels of indoor light and also typical spectra from neonatal lamp sources.

4.2. Suitability of NewBorn Anne manikin

The NewBorn Anne manikin provided a useful device for experimental observations of neonatal lamp outputs with surface areas of anatomical areas matching those of term neonates. Useful possible enhancements would include flexible knee joints to allow measurement of 'straight' legs from both overhead and blanket type phototherapy light sources. The raised knee of the NewBorn Anne 'babyshape' also reduced the effective surface area of light incident at right angles to the lower leg surfaces and would likely also not efficiently detect light from blanket systems.

4.3. Suitable spectra for use of 'babyshape' detection system

While the spectral response of the measured series of PowerFilm solar elements is narrower than comparable elements designed for solar power applications, there remained significant sensitivity to spectral outputs in region 500 nm to 700 nm which was notionally outside the perceived range of therapeutic wavelengths of neonatal phototherapy. It was considered desirable to reduce background light levels to less than around 50 lux when making output measurements of neonatal lamp sources with the 'babyshape' system.

In addition, non-therapeutic illumination from neonatal phototherapy lamp units should, if possible, be disabled in order that only the therapeutic wavelengths typically less than 500 nm from LEDs are detected. The system would not be suitable for use with white light sources, including sunlight where the detection signal from therapeutic neonatal phototherapy wavelength ranges would be overwhelmed by the extended non-therapeutic wavelengths. It would be desirable to include the option of suppression of supportive non-therapeutic illumination in future specifications of neonatal phototherapy devices.

4.4. Clinical application of dose rate information

The ability to track the dose rate of delivered therapeutic optical radiation during neonatal phototherapy provides a new parameter which has the potential to assist in the treatment of hyperbilirubinemia. Two key sets of associated measurements are identified, one being that of neonate serum bilirubin in values of μmole litre^{-1} as advised in NICE framework [12] at specified date/times and the other the estimated delivered optical energy of phototherapy treatment light between identified date/time values within a specified optical waveband such as those described as AAP2004 and AAP2011. A relevant and as yet unsubstantiated consideration, however, is that in the time period of clinical management of neonatal phototherapy, changes in the structural characteristics of the neonate skin may result in changes in the fractional spectral component of light actively involved in bilirubin reduction [13].

In a notional example of levels of absorbed dose, an AAP2011 value of 40 μW cm^{-2} nm^{-1} is equivalent to an irradiance value of 1.2 mWcm-^{2} which over a typically exposed surface of a term neonate of 650 cm^2 is equivalent to around 800 mW. A more detailed value would be available from data from use of the 'babyshape' system. Thus in a 4 hour interval of neonatal phototherapy, at this notional rate, the delivered dose would be 11.52 kJ. The data set of bilirubin values is essentially part of existing routine clinical observation.

Key additional data for analysis is the value of estimated gestation at birth in whole weeks (23 to >=38), the birth weight of the neonate and the date/time of birth to link with the corresponding NICE nomogram

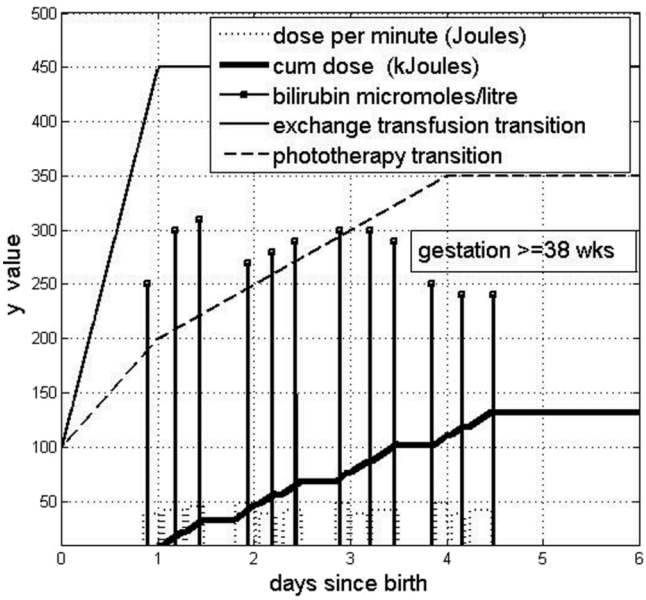

Fig. 12. Representation of the potential role of estimated dose rate values in management of neonatal phototherapy.

chart which identifies specific areas of risk in relation to serum bilirubin levels. In this mode, the time origin is referenced to time since birth in units of elapsed days. Fig. 12 indicates a notional representation of the potential role of estimated dose rate values of neonatal phototherapy in clinical management of the neonate for a gestational age of >=38 weeks where data was entered in an Excel file and calculations made using a MATLAB programme. In this simulated case history, the neonate enters the status area of indication for phototherapy and following phototherapy the bilirubin revels revert to values in the normal range. It is planned to observe such relationships in a pilot clinical study.

While a visual representation of parameter trends is of benefit, the

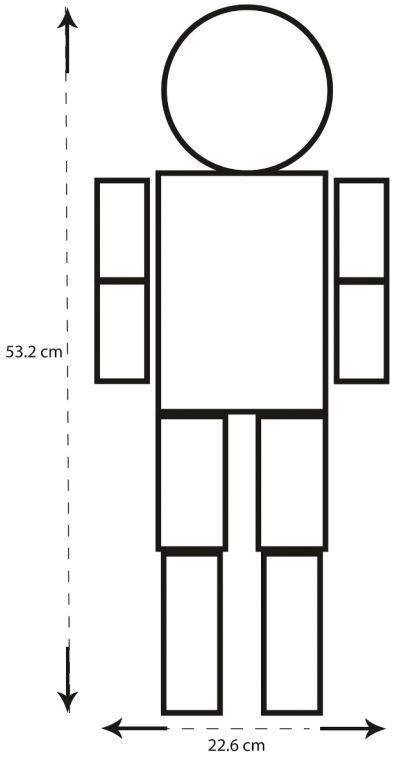

Fig. 13. Representation of 'Cindy'.

data can potentially provide additional information to assist the clinical management of hyperbilirubinemia. In the case, for example, of reduction of bilirubin over the time period of phototherapy, this provides an indication of change of bilirubin values for a given energy dose and where relevant units would be μmole litre^{-1} kJ^{-1} and would represent a clinical parameter of some relevance, essentially as a measure of the clinical response to neonatal phototherapy. In addition a linked parameter factoring in the weight of the neonate at birth would be expressed in units of μmole litre^{-1} kJ^{-1} kg^{-1} .

In terms of improved management of the process of phototherapy, derived parameters could include a predicted trajectory of bilirubin values based on available data sets and also a recommended phototherapy dose rate for a desirable treatment trajectory. While these are desirable parameters, it is unclear if they can be reliably determined.

4.5. Towards measurement standards

As often encountered in the field of medical devices, there can often be a lack of suitable test equipment to adequately verify output therapeutic parameters of equipment. IEC medical device standards [14] tend to focus on aspects of electrical safety and constructional details rather than on more specialist aspects of therapeutic output levels.

It is desirable to work towards test systems of accepted design that can usefully estimate the delivered power during neonatal phototherapy over a neonate surface of specific gestational maturity. A first step in this direction would be the adoption of standard 'babyshape' constructs that essentially replicated the equivalent real world anatomical profiles of neonates at identified gestational ages. Fig. 13 indicates an initial notional construct for a term manikin based on the surface areas of the NewBorn Anne unit. In a first approximation of a new manikin (Cindy), the head is a solid sphere and other elements solid cylinders including the main torso section. The notional light sensing surfaces on the cylinder sections are assumed to be the curved surfaces. Degrees of movement of legs and arm section require consideration.

The specification of the sensing technology would be more complex, though it may be more appropriate to focus on aspects of measurement performance rather than define a specific light sensing product. Considerations could include useful wavelength sensitivity range, variation of sensitivity with temperature, degree of cosine response conformity and stability of sensitivity to light exposure. In addition it would be relevant to specify values of percentage active sensing area on each designated anatomical area. An 'essential' value of 75 % is suggested and with a target value of 90 %. Observed values using the 'babyshape' will also be influenced by, for example, the reflectivity characteristics of the material on which the 'babyshape' rests and in a standard test configuration would require definition.

5. Conclusion

A system is described which can provide detailed information on the output delivered power distribution from neonatal phototherapy sources, which can improve their design and allow for more effective management of hyperbilirubinemia. In addition, the identified measurement technology indicates the potential for development of associated testing standards for the output power distribution of such devices.

CRediT authorship contribution statement

D.M. Clarkson: Conceptualization, Data curation, Formal analysis, Investigation, Methodology, Project administration, Resources, Software, Validation. **P. Satodia:** Conceptualization, Project administration, Resources, Funding acquisition.

Acknowledgements

The assistance is acknowledged of Professor Adrian Wilson of Department of Research and Development at UHCW NHS Trust in practical aspects of logistics and scientific and technical support. Also on going organisational support from Ceri Jones, Head of Research, Development and Innovation at UHCW NHS Trust is acknowledged. The assistance of Belmont Medical Technologies Ltd in providing the loan of the NeoBLUE unit is acknowledged.

References

[1] D.M. Clarkson, M. Tshangini, P. Satodia, Preliminary observations of a system for determination of phototherapy exposure over a neonate body shape, Med. Eng. Phys. 95 (2021) 1–8. -Sep.
[2] G.B. Haycock, G.J. Schwartz, D.H. Wisotsky, Geometric method for measuring body surface area: a height-weight formula validated in infants, children, and adults, J. Pediatr. 93 (1) (1978) 62–66. -Jul.
[3] E.A. Gehan, S.L. George, Estimation of human body surface area from height and weight, Cancer Chemother. Rep. 54 (4) (1970) 225–235.
[4] A.S. Al-Ezzi, M.N.M. Nainar, Photovoltaic Solar Cells: a Review, Appl. Syst. Innov. 5 (4) (2002) 67, https://doi.org/10.3390/asi5040067.
[5] D.M. Clarkson, R. Nicol, P. Chapman, Neonatal phototherapy radiometers: current performance characteristics and future requirements, Med. Eng. Phys. 36 (4) (2014) 522–529. -Apr.
[6] D.M. Clarkson, P. Satodia, Use of a hand-held spectroradiometer for the measurement of neonatal phototherapy lamp outputs, Med. Eng. Phys. 73 (2019) 107–111. -Nov.
[7] American Academy of Pediatrics Subcommittee on Hyperbilirubinemia, Management of hyperbilirubinemia in the newborn infant 35 or more weeks of gestation, Pediatrics 114 (1) (2004) 297–316. -Jul.
[8] V.K. Bhutani, Committee on Fetus and Newborn; American Academy of Pediatrics. Phototherapy to prevent severe neonatal hyperbilirubinemia in the newborn infant 35 or more weeks of gestation, Pediatrics 128 (4) (2011) e1046–e1052.
[9] B. Rech, H. Wagner, Potential of amorphous silicon for solar cells, Appl. Phys. A 69 (1999) 155–167.
[10] M. Fehr, A. Schnegg, B. Rech, O. Astakho, F. Finger, R. Bittl, et al., Metastable defect formation at microvoids identified as a source of light-induced degradation in a-Si:H, Phys. Rev. Lett. (2014), https://doi.org/10.1103/PhysRevLett.112.066403.
[11] C.R. Wronski, The Staebler-Wronski Effect, editor, in: JI Pankove (Ed.), Semiconductors and Semimetals, Elsevier, Amsterdam, 1984, pp. 347–374.
[12] Jaundice in Newborn Babies Under 28 Days Clinical guideline, 2023 [CG98] Published: 19 May 2010 Last updated: 31 October 2023: https://www.nice.org.uk/guidance/cg98/resources [accessed 19 December 2023].
[13] L. Finlayson, I.R.M. Barnard, L. McMillan, S.H. Ibbotson, C.T.A. Brown, E. Eadie, et al., Depth penetration of light into skin as a function of wavelength from 200 to 1000 nm, Photochem. Photobiol. 98 (4) (2022) 974–981. -Jul.
[14] IEC 60601-2-50:2020+AMD1:2023 CSV, Medical electrical equipment - Part 2-50: particular requirements for the basic safety and essential performance of infant phototherapy equipment, 2023, Geneva.